TECHNICAL MEMORANDUM

618

Direct 4D-Var assimilation of all-sky radiances. Part I: Implementation

Peter Bauer, Alan J. Geer, Philippe Lopez and Deborah Salmond

Research Department

Submitted to Quart. J. Roy. Meteorol. Soc.

April 2010

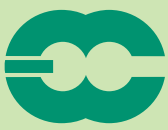

European Centre for Medium-Range Weather Forecasts
Europäisches Zentrum für mittelfristige Wettervorhersage
Centre européen pour les prévisions météorologiques à moyen terme

Series: ECMWF Technical Memoranda

A full list of ECMWF Publications can be found on our web site under:
http://www.ecmwf.int/publications/

Contact: library@ecmwf.int

European Centre for Medium-Range Weather Forecasts
Shinfield Park, Reading, RG2 9AX, England

Abstract

This paper describes a new radiance assimilation scheme for microwave imager observations which unifies the treatment of clear-sky, cloud and precipitation-affected situations, giving an 'all-sky' approach. The previous approach assimilated radiances in clear skies and retrievals of total column water vapour in clouds and rain. In March 2009, the new approach became operational in the Four-Dimensional Variational Assimilation (4D-Var) system of the European Centre for Medium-Range Weather Forecasts. This approach employs moist physics parameterizations and a full multiple scattering radiative transfer model in the observation operator for all microwave imager observations. Observation operator accuracy, observation error definition and bias correction, basic observational impact, 4D-Var linearity and stability as well as computational cost are described. Because of careful quality control and relatively large observation errors, the all-sky system produces a weaker observational constraint on moisture analysis than the previous system. However, in single-observation experiments where the observations are given the same weight as before, the all-sky system is able to produce 4D-Var analyses that are closer to the observations than the previous approach. Despite the nonlinearity of rain and cloud processes, 4D-Var minimises successfully through the use of an incremental technique. Overall the quality of the 4D-Var minimisation, in terms of number of iterations and conditioning, is unaffected by the new approach.

1 Introduction

Today's forecasting models operate at 15-25 km on global scales, and 1-3 km on regional scales, with an unprecedented accuracy of temperature and wind forecasts but still limited accuracy when forecasting precipitation. The spatial scale at which numerical models exhibit acceptable precipitation forecast skill is much coarser than the nominal model resolution and even that skill is highly dependent on how localised the rain structures are (Roberts and Dean, 2008).

In global Numerical Weather Prediction (NWP) systems, satellite observations provide 90-95% of the actively assimilated data. However, over 75% of satellite observations are discarded due to cloud contamination and unknown land, snow and sea-ice surface emissivity. Cloud-affected data is difficult to deal with because of the limited accuracy of moist physics parameterizations in numerical models and the need to model radiative transfer through clouds and precipitation. Modern data assimilation approaches such as Four Dimensional Variational Assimilation (4D-Var) and ensemble methods are geared towards clear-sky data. In particular, the modelling of dry processes and their error characteristics is much better developed than for moisture and cloud processes.

Over the last 20 years, the assimilation of precipitation has been developed from physical initialisation (Krishnamurti *et al.*, 1984) to four-dimensional variational assimilation schemes (e.g. Županski and Mesinger, 1995). Rainfall observations are assimilated at a number of operational centres, with Japan Meteorological Agency (JMA) assimilating ground-based radar data into a regional model using 4D-Var (Tsuyuki *et al.*, 2002) and the National Centre for Environmental Prediction (NCEP) assimilating satellite retrievals into a global model using 3D-Var (Treadon *et al.*, 2002). At the European Centre for Medium-Range Weather Forecasts (ECMWF), the assimilation of rain-affected microwave radiances became operational in 2005 (Bauer *et al.*, 2006a,b). The latter represented the first global 4D-Var system in which rain observations were routinely assimilated.

Errico *et al.* (2007) summarise the most important issues related to the assimilation of cloud and precipitation observations and conclude that since there is very little experience with data assimilation of observations related to moist processes, much fundamental evaluation of suitability and performance of existing data assimilation systems will have to be performed. One prominent problem is the non-linearity (and non-continuity) of models, i.e. the sensitivity of the parameterizations to input parameter perturbations is strongly state dependent. In the case of strong non-linearities, data assimilation may produce erroneous analysis increments in model state

variables. This in turn may affect balance and stability. Another problem is the lack of investigation into observation and background errors in cloudy and rainy situations.

In an idealised modelling framework, Vukicevic and Posselt (2008) evaluated the dependence of the data assimilation solution on model non-linearity (and non-monotonicity) and emphasised the risk of finding non-unique solutions (i.e. non-optimal analyses). This risk is greatly increased if model errors are significant but it can be decreased by the cumulative impact of independent observations. An explicit test of the correspondence between non-linear and linearised model physics has been performed by Amerault *et al.* (2008) with a meso-scale model. They concluded that the tangent-linear approximation was sufficiently accurate for forecasts up to 1 hour. For global models this range and therefore the assessment of the validity of the tangent-linear approximation is more complicated due to the general use of different model resolutions and time steps as well as different physical parameterizations in outer-loop (non-linear) and inner-loop (linearised and regularised) calculations employed at most operational centres (Andersson *et al.*, 2005).

Observation and background errors are difficult to quantify due to the complexity of the processes involved. Also the errors may be strongly state dependent and may not be represented by general Gaussian statistics. Observation (operator) errors are mainly driven by the representativeness error and the fundamental assumptions used in radiative transfer (RT) modelling (Amerault and Zou, 2003). The representativeness errors relate to the spatial representation of sub-grid-scale variability in the model versus that of observation. Often, for computational performance reasons, very simple parameterizations have to be used, e.g. defining an effective cloud/precipitation coverage fraction that minimises radiative transfer errors when validated against observations (Geer *et al.*, 2009).

Moreau *et al.* (2004) and Bauer *et al.* (2006a) have shown that for global models it is preferable to assimilate microwave radiances rather than rain rates because:

- the observation operator always produces non-zero gradients (in the absence of signal saturation) whether a scene contains clouds or not;
- an observation operator which combines moist physics and radiative transfer model behaves more continuously over its dynamic range than does moist physics alone;
- the statistics of observed-minus-modelled radiance departures have mostly Gaussian characteristics, and this also facilitates bias correction;
- observation operator errors can be derived from spatial departure covariance statistics.

The background error definition depends on the control variables used in the assimilation scheme. In earlier studies on 1D-Var retrievals of hydrometeor profiles from radiance observations where the observation operator consisted only of the RT model, hydrometeor background errors could be calculated from the state-dependent temperature and humidity background errors to which the moist physics operator was applied (Moreau *et al.*, 2003). The temperature and humidity background errors, however, did not take account of the presence of clear skies or cloud. Amerault and Zou (2006) derived background error statistics at the meso-scale from the statistical difference between parameterization schemes assuming that those represent realistic parameterization errors. The main challenge here is to define a simple yet accurate scheme that allows a state-dependent error definition in an operational environment. In the future, ensemble data assimilation may be one way to obtain more realistic background errors than currently available. These methods are currently being developed and promise to provide better statistics and a more balanced weight between model forecasts and observations in the analysis.

This paper and its companion (Geer *et al.*, 2010b) describe improvements in the use of microwave satellite observations in the ECMWF forecasting system. Since March 2009, the operational system has assimilated

all-sky microwave radiances directly into 4D-Var. The current paper describes the rationale behind the all-sky approach and the technical details of the implementation. It examines the system using single-observation test cases and looks at issues such as the non-linearity of the observation operator, and the convergence and numerical performance of the full system. The second paper examines the use of all-sky observations in the context of the full ECMWF operational system by looking at analysis and forecast skill.

2 Assimilation system

2.1 Overview

Rain and cloud assimilation is incorporated within the ECMWF's 4D-Var system (Rabier *et al.*, 2000), alongside the assimilation of many other conventional and satellite observation types. 4D-Var seeks to make the best estimate or 'analysis' of the atmospheric state $\mathbf{x}(t_0)$ at time t_0 by minimising a cost-function:

$$\begin{aligned} J[\mathbf{x}(t_0)] &= \frac{1}{2}[\mathbf{x}(t_0)-\mathbf{x}^{\mathrm{b}}(t_0)]^{\mathrm{T}}\mathbf{B}_0^{-1}[\mathbf{x}(t_0)-\mathbf{x}^{\mathrm{b}}(t_0)] \\ &+ \frac{1}{2}\sum_{i=0}^{n}\mathbf{d}_{\mathrm{i}}^{\mathrm{T}}\mathbf{R}_{\mathrm{i}}^{-1}\mathbf{d}_{\mathrm{i}} \end{aligned} \tag{1}$$

For full definitions see Ide *et al.* (1997); for more explanation see Kalnay (2003). A first guess (FG) model forecast $\mathbf{x}^{\mathrm{b}}(t_0)$ provides a background. Observations are distributed within a time window (in our case 12 hours) divided into n discrete timeslots i. In each timeslot, observations $\mathbf{y}_{\mathrm{i}}^{\mathrm{o}}$ are compared to the corresponding model estimates to calculate the 'departure' of model from observation:

$$\mathbf{d}_{\mathrm{i}} = \mathbf{y}_{\mathrm{i}}^{\mathrm{o}} - H_i[M_i[\mathbf{x}(t_0)]] \tag{2}$$

H_i is a non-linear 'observation operator' that, for example, simulates observed brightness temperature (TB) given input values from the atmospheric model. $M_i[\mathbf{x}(t_0)]$ represents running the non-linear atmospheric model from timestep t_0 to t_i. The weighting between background and observations and the spreading of the observational information in space are determined by the choice of background and observation error covariance matrices, $\mathbf{B}$ and $\mathbf{R}_{\mathrm{i}}$.

It is useful to distinguish between the 'control vector', i.e. the part of $\mathbf{x}(t_0)$ that is varied in order to minimise the cost function, and other atmospheric or surface state variables, which may either be held fixed or be derived from the variables in the control vector. In the ECMWF system, the control vector contains only quantities related to winds, temperature, moisture and surface pressure, i.e. there is no cloud or precipitation in the control vector. Some other quantities, such as sea surface temperatures and surface parameters, are held fixed. However, cloud and precipitation are derived from the clear atmospheric variables by the application of moist physics operators as part of the atmospheric model M_i, and hence cloud and precipitation must still be optimised in 4D-Var if cloud- or rain-affected observations are assimilated.

To make the cost function into an 'easily' soluble quadratic form, the non-linear operators H_i and M_i in Eq. 2 are replaced by tangent linear operators $\mathbf{H}$ and $\mathbf{M}$, which are the matrices of the partial derivatives of H_i and M_i. Whether the linear solution is valid depends on the validity of the tangent linear hypothesis, for example for $\mathbf{M}$:

$$M_i[\mathbf{x}(t_0)+\delta\mathbf{x}\,] \simeq M_i[\mathbf{x}(t_0)] + \mathbf{M}_i\delta\mathbf{x}, \tag{3}$$

and similarly for $\mathbf{H}$. for The cost function, once in quadratic form, can be minimised using an iterative algorithm which, at each step, requires a calculation of the cost function and its gradient. Calculation of the gradient requires the use of 'adjoint' operators, which are the transposes $\mathbf{H}^{\mathrm{T}}$ and $\mathbf{M}^{\mathrm{T}}$.

In practice, the basic version of the cost function is extended in various ways. Quality control is applied by scaling the cost function according to each observation's probability of gross error (Variational Quality Control, VarQC; Ingleby and Lorenc, 1993; Andersson and Järvinen, 1998). The control vector is augmented to allow the estimation of parameters for the correction of observation biases (Variational Bias Correction, VarBC; Dee, 2004; Auligné *et al.*, 2007).

ECMWF also use an incremental formulation for the minimisation (Courtier *et al.*, 1994), based around a non-linear 'outer-loop' update and a linearised 'inner-loop' minimisation. After each outer-loop, the linearisation point about which **H** and **M** are calculated is updated. The idea is that the linearisation point gets closer to the eventual analysis and the tangent linear assumption becomes gradually more valid. The outer loop steps are run with the atmospheric model using a spectral resolution of T799 (or sometimes T511 for computational efficiency in our tests here). There are three runs of the inner-loop, all at a reduced resolution, the first at T95, the second at T159, and the third at T255. We will explain these concepts in more detail later.

2.2 Observations

Microwave imagers typically have a number of channels between 10 GHz and 89 GHz. Outside of heavy precipitation and cloud, the atmosphere is usually semi-transparent at these frequencies. Due to the difficulties of modelling land surface emissivities and temperatures, we only use these observations over ocean surfaces. Here, observed TBs are sensitive to the sea surface (skin temperature and wind speed) and the atmosphere (water vapour, cloud and precipitation). The emissivity of the sea surface is typically much less than 1 and so the surface typically provides a cool background against which water vapour, clouds and rain show up as warm emitters. However, at higher frequencies, TBs can decrease with increasing moisture or cloud, either due to scattering from frozen hydrometeors or to the weighting function moving to higher, relatively cool parts of the atmosphere. Microwave imagers use a conically-scanning technique where all observations have the same zenith angle and (for a particular frequency) footprint size.

The ECMWF all-sky system uses observations from Special Sensor Microwave / Imager (SSM/I) and Advanced Microwave Scanning Radiometer for the Earth Observing System (AMSR-E). SSM/I instruments have been flown on the Defence Meteorological Satellite Program (DMSP) satellites from 1987 until the present day (Hollinger *et al.*, 1990). Here we use observations from DMSP-F13 and F15. SSM/I has seven channels from 19 GHz through to 85 GHz, labelled by their frequency plus a 'v' or 'h' depending on their polarisation (vertical or horizontal): 19v, 19h, 22v, 37v, 37h, 85v and 85h. AMSR-E (Kawanishi *et al.*, 2003) provides channels 7v/h, 10v/h, 19v/h, 24v/h, 37v/h and 89v/h, but here we avoid the 7 and 10 GHz channels due to problems with our surface emissivity modelling at low frequencies and the 89 GHz channels since they are not spatially co-registered with the lower frequency channels.

Tropical Rainfall Measuring Mission (TRMM) Microwave Imager (TMI) and Special Sensor Microwave Imager Sounder (SSMIS) were assimilated in the previous ECMWF system but to save computer resources, their use has been temporarily discontinued (Sect. 6.3).

2.3 Observation operator

RTTOV-SCATT (Bauer *et al.*, 2006c) provides multiple-scattering radiative transfer calculations at microwave frequencies as part of the RTTOV[1] package (Eyre, 1991; Saunders, 2008). Scattering calculations are performed using the delta-Eddington approach (Joseph *et al.*, 1976), which gives reasonable results when simulating the radiances measured by microwave radiometers (Smith *et al.*, 2002). Scattering parameters are pre-calculated

[1] Radiative Transfer model for Television Infrared Observation Satellite Operational Vertical sounder

using Mie theory and tabulated as a function of frequency, temperature, and hydrometeor type and density. The most important inputs to RTTOV-SCATT are the surface skin temperature and winds, and vertical profiles of pressure, temperature, moisture, cloud liquid water and ice, rain and snow fluxes, and cloud cover. We use the revised cloud overlap approach of Geer *et al.* (2009), which results in substantially more accurate cloudy and rainy radiative transfer than with previous versions of RTTOV-SCATT.

3 Previous approach: 1D+4D-Var

The system that was implemented at ECMWF in June 2005 (Bauer *et al.*, 2006a,b) consisted of two stages. First, SSM/I radiance observations were used to constrain a one-dimensional variational (1D-Var) retrieval of total column water vapour (TCWV). Then, the TCWV was assimilated as a pseudo-observation in 4D-Var. This was known as '1D+4D-Var'. Separately, clear-sky SSM/I observations were assimilated directly into 4D-Var. Further developments to the 1D+4D-Var system were described by Geer *et al.* (2008) and in June 2008, rain and cloud-affected observations from AMSR-E and TMI were included.

What distinguishes 1D-Var from an ordinary variational retrieval is (a) it uses the same background state and temperature and moisture background errors as the 4D-Var and (b) the observation operator uses the same linearised moist physics package as the 4D-Var. The control vector consists of temperature and moisture profiles. Fixed information includes the background temperature and moisture tendencies, latent and sensible heat flux at the sea surface. With this as input, the observation operator consists of (i) linearised moist physics parameterizations (Tompkins and Janisková, 2004; Lopez and Moreau, 2005), which are used to derive the cloud and precipitation profiles and (ii) RTTOV-SCATT, which is used to calculate the microwave radiances. An advantage of doing a 1D-Var retrieval is that it allows an additional step of quality control before assimilation into 4D-Var.

One of the main recent improvements was the correction of a bias in the linearised moist physics parameterizations, which were producing excessive rainfall compared both to the non-linear parameterization on which they were based, and compared to independent rain observations (Geer *et al.*, 2008). This highlights the importance in rain and cloud assimilation of using a model that is able to accurately predict rain and cloud amounts.

Geer *et al.* also noted a number of limitations of the 1D+4D-Var approach. First, the TCWV pseudo-observation was not bringing that much new information: much of the 4D-Var analysis humidity increment is inferred indirectly from other observations, such as temperature-sounding radiances. The unique information content of the microwave imager observations was in their cloud and rain information. Rather than discard this, it would be better to make use of it in a direct 4D-Var assimilation of radiances. Second, the separate treatment of clear-sky and cloud/rain-affected observations created an unbalanced sampling. Cases with clear observations but a cloudy first guess went through the clear sky route, using clear-sky radiative transfer in the observation operator. This meant that (a) there was quite a large sampling bias in the 1D+4D-Var stream and (b) an opportunity was being missed to correct the erroneous FG cloud when clear skies were observed. An all-sky approach was proposed, where the treatment of clear and cloud-affected cases is unified in a single data stream with a single observation operator. This is what is implemented in this paper.

One final problem was that near saturation the background error definition tends to penalise positive moisture increments more strongly than negative increments. This means that the assimilation of rain and cloud affected data causes a net drying effect on the moisture analysis. However, this issue is not addressed by the new system, and remains a problem (Geer *et al.*, 2010b). In the future, it can only be overcome by extending the 4D-Var control vector and background errors to include condensates.

4 All-sky approach

4.1 Introduction

The all-sky approach is best introduced by explaining how it differs from the treatment of clear-sky radiance data. At ECMWF, the following steps usually take place:

1. Observations are thinned by scan-line and scan-position;
2. Model fields are interpolated to observation locations;
3. Observations are simulated using a clear-sky radiative transfer model;
4. A bias-correction is applied, based on the VarBC estimate from the previous analysis;
5. Cloud-affected observations are removed;
6. A FG departure check (BgQC) is performed for quality control;
7. Data is further thinned by time slot onto a latitude-longitude grid to avoid spatial and temporal correlation of observation (operator) errors;
8. Observation errors are pre-defined and remain constant throughout the analysis. They are not model-state dependent.
9. VarQC operates through the minimisation for further quality control;

The all-sky approach is completely different except for steps 4, 6, 7 and 9.

There is no spatial interpolation in the all-sky assimilation. Interpolating fields from the moist physics model output to observation locations was considered inappropriate due to the large horizontal variability and the potential loss of physical consistency among profiles of temperature, humidity, hydrometeor contents and surface parameters. Consistency is only guaranteed at each model grid point. The difficulty comes particularly from the high sensitivity of convection parameterizations to input perturbations. In the all-sky approach, the radiative transfer model (and its tangent-linear and adjoint) is run only at grid point locations. In order to reduce the geographical mismatch to a minimum, we only use observations that are less than 10 km from the grid points, and (for each sensor) only one observation per grid point. Hence, there is no need for further thinning or interpolation, so steps 1 and 2 are eliminated. As previously mentioned, step 3 now uses a scattering radiative transfer model to allow computations in cloud and precipitation.

The all-sky treatment unifies clear-sky and cloud-affected observations and has a single observation operator. Thus, there is no longer any cloud detection involved, eliminating step 5. This gives the major advantage of a balanced sampling. Figure 1 shows histograms of FG departures for the seven channels on SSM/I. Individual curves have been drawn for those data samples where both model and observations contain clouds (dotted, 37%) or only clear-sky (solid, 35%), where the observations contain clouds but the model is cloud-free (dash-dotted, 11%) and vice versa (dashed, 17%). Figure 2 shows the corresponding geographical distribution of the samples.

The clear-sky approach allows the sum of the solid and dashed samples into the analysis, the latter being about half the size of the former. The geographical distribution suggests that many areas in which cloud is different between observations and model are located near fronts and convective systems that are slightly

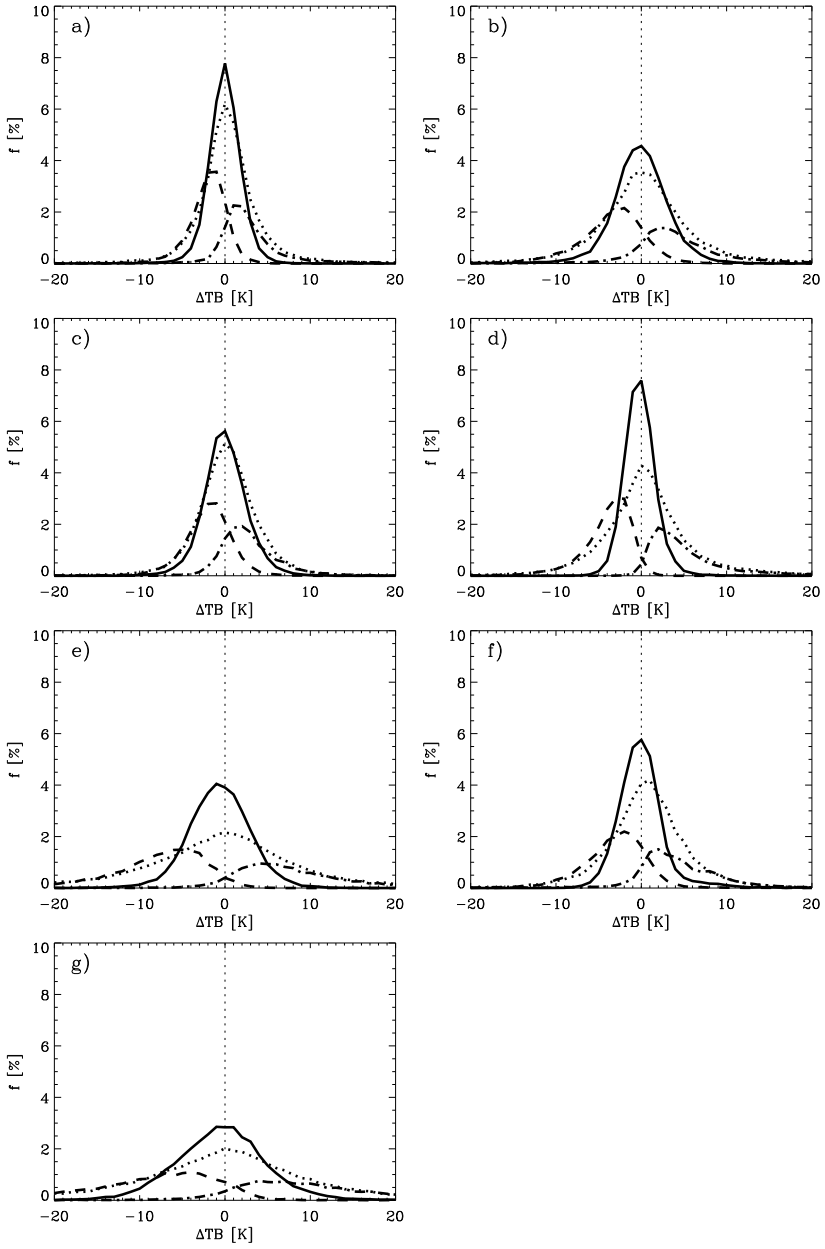

Figure 1: Histograms of SSM/I first-guess radiance departures for samples where both model and observations contain clouds (dotted) or only clear-sky (solid), where the observations contain clouds but the model is cloud-free (dash-dotted) and vice versa (dashed) for channels 19v (a), 19h (b), 22v (c), 37v (d), 37h (e), 85v (f), 85h (g). Data drawn from a 12-hour assimilation on 15 September 2007 00 UTC.

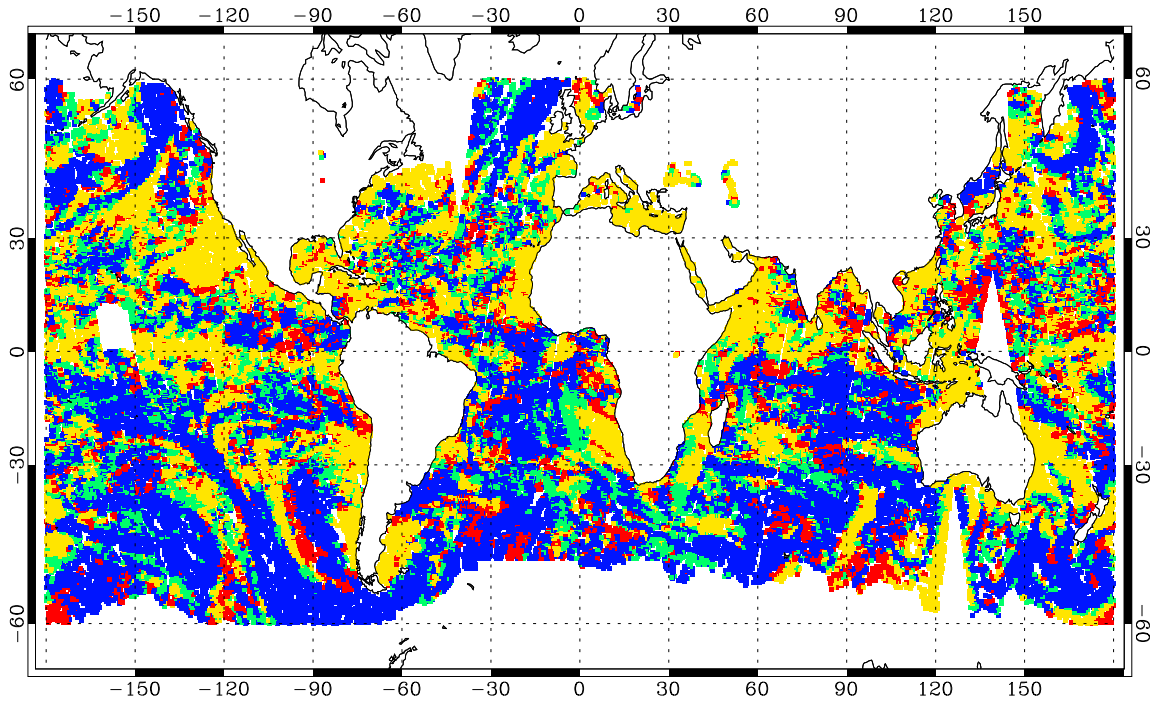

Figure 2: Geographical distribution of SSM/I data from a 12-hour assimilation on 15 September 2007 00 UTC for samples where both model and observations contain clouds (blue) or only clear-sky (yellow), where the observations contain clouds but the model is cloud-free (red) and vice versa (green).

misplaced by the model but where the cloud extent is well represented by the model. In those cases, the clear-sky radiance assimilation would introduce increments only on the side of the system where the observations are clear. However, the all-sky system is able to develop model clouds where there are none in the first guess and to dissipate model clouds if there are none in the observations. In total, 65% of observations are affected by cloud either in the model or observation, and many of the remaining 35% of supposedly clear observations may be affected by small amounts of cloud.

Figures 1a-g also suggest that the biases in radiance space are small for the samples where both model and observation agree in terms of cloud. This suggests that both clear-sky and cloud observation operators perform well across all SSM/I channels and that the bias correction is correctly adjusting for any remaining systematic differences on a global basis.

Steps 4 (bias correction) and 6 (FG departure check) are retained for the all-sky system and are described in Secs. 4.3 and 4.4 respectively. In the all-sky system, it is clear that observation errors are likely to be larger in rain and cloud affected areas, due to the increased difficulty of modelling these phenomena. Thus a completely new approach to the definition of observation errors (step 8) is needed. This is described in Sec. 4.2. It is also necessary for the first time to really consider the spatial representativeness of observations (Sec. 4.5).

4.2 Observation errors

Observation errors are allowed to vary through the minimisation and are scaled depending on: (a) the total hydrometeor amount in the FG; (b) the distance of the observation from the nearest model grid point. From previous work we know that observation errors are generally larger in cloud and rain. The true instrument noise is irrelevant here; it is representativity (or lack of it) and observation operator error that is important. For

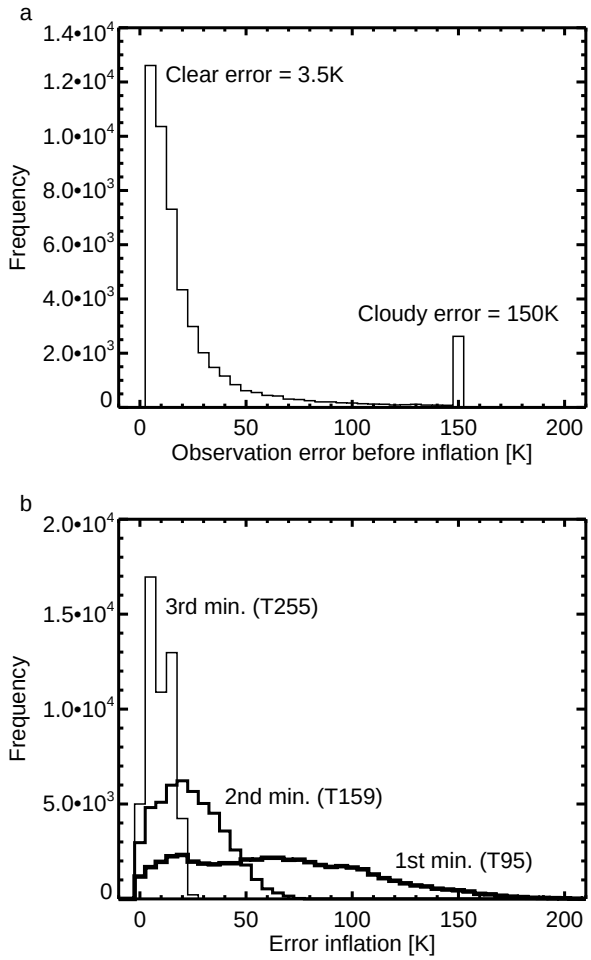

Figure 3: (a) Histogram of observation errors for channel 37v, before inflation; (b) Histogram of the additional inflation term, proportional to the square of the distance from the grid point ($(r/r_c)^2$), which changes depending on the resolution of the minimisation. Sample is all assimilated SSM/I observations at 00Z 22nd August.

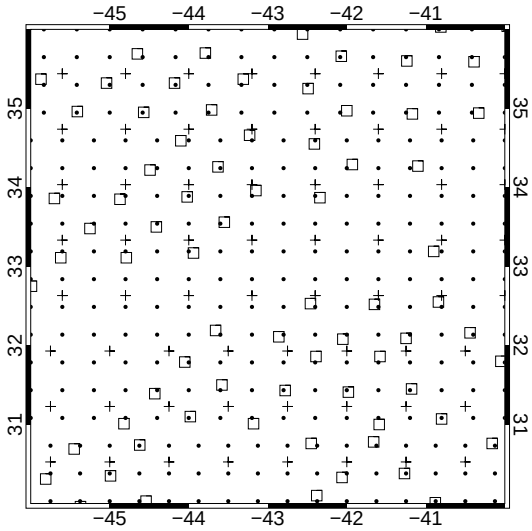

Figure 4: Map of SSM/I observations (squares), outer-loop T511 grid-points (dots) and final inner-loop T255 grid-points (crosses). SSM/I observations are selected on the basis of being less than 10 km from the outer-loop grid-point, but only every second grid-point is used, to help thin the data. Co-ordinates are latitude and longitude in degrees. The squares are symbolic and do not represent the observation resolution.

example, the accuracy of scattering radiative transfer is typically lower than for clear sky (see e.g. Geer *et al.*, 2009, errors could be 10 times bigger in cloud). For each channel, a clear sky error σ_o^{clr} and a cloudy/rainy sky error σ_o^{cld} are defined. The nominal observation error $\sigma_{o,n}$ is determined from:

$$\sigma_{o,n} = c\sigma_o^{clr} + (1-c)\sigma_o^{cld} \tag{4}$$

but with the clear and cloudy errors providing upper and lower bounds:

$$\sigma_o^{clr} < \sigma_{o,n} < \sigma_o^{cld} \tag{5}$$

Here c is the total column hydrometeor amount in the model, in kg m^{-2}. This is the sum of cloud water path (CWP), ice (IWP), rain (RWP) and snow (SWP). The model represents snow and rain in terms of fluxes, so the densities needed to calculate RWP and SWP are derived using a transformation described by Geer *et al.* (2008). The nominal error is allowed to vary through the minimisation, thus accounting for the potential generation and dissipation of clouds. Figure 3a shows a typical histogram of nominal observation errors for channel 37v.

Observation errors for SSM/I were calculated as in Bauer *et al.* (2006a) from spatial departure covariance statistics and were defined in clear skies as σ_o^{clr} = 3, 4.5, 4, 3.5, 4 K (19v, 19h, 22v, 37v, 85v) and in cloudy skies σ_o^{cld} = 3, 6, 3, 150, 300 K. At high frequencies we artificially inflated the observation error in cloudy situations to prevent assimilation. This is because, compared to lower frequencies, there is increasing sensitivity to frozen precipitation, which is less well modelled by the moist physics parameterizations. Also, the optical properties of frozen hydrometeors are less well known, making radiative transfer more difficult. For this reason Bauer *et al.* (2006a) only assimilated channels at 19.35 and 22.235 GHz in the 1D+4D-Var system. Channels 37h and 85h were found to be too strongly affected by surface emissivity modelling biases and were therefore excluded in both clear and cloudy skies. The smaller error at 22.235 GHz in clouds is explained by the much reduced dynamic range of radiances due to water vapour absorption. Note that it is assumed that errors are spatially and spectrally uncorrelated.

To the nominal observation error is added an 'inflation term' to account for the distance r between the observation and the model grid-point. This is needed because the model resolution changes at each inner-loop of

4D-Var and is different from the outer-loop resolution. This means that r will also change (e.g. Fig. 4). We assume that as r increases, the observation becomes less representative of the grid-box in which it is being assimilated. The nominal observation error is inflated quadratically so that the final observation error is:

$$\sigma_o = \sigma_{o,n} + (r/r_c)^2. \tag{6}$$

Here, r_c =10 km is a critical radius, at which the inflation term is 1 K.

The inflation of error with distance means that while the same number of observations is retained throughout the minimisation, the observation weight is adjusted. When at higher model resolution the observations are more likely to be close to a grid-point, so the observational weight increases. Figure 3b shows histograms of the inflation term at the three different minimisation resolutions. Observations are typically given very large errors during the first and second minimisations. This reduces the risk of too strong increments in the initial coarse-resolution minimisations where the tangent-linear approximation with active moist physics is most likely to be false.

4.3 Quality control

It is important to screen out bad or outlying observations which might otherwise significantly degrade the quality of the analysis, and this process is known as quality control (QC). With rain and cloud-affected observations, QC is challenging, since it is perfectly normal to, for example, find a situation with a rainy FG and a clear-sky observation. In such cases, FG departures could easily be as large as 50 K. In a traditional clear-sky QC approach, a large FG departure indicates a bad observation, which would be rejected. In our initial implementation of the All-Sky approach, this problem remains, because we apply the standard Background QC (BgQC Järvinen and Unden, 1997) which actually does reject such 'valid' observations.

BgQC rejects observations where the FG departure is greater than a factor α times its estimated error standard deviation, i.e:

$$d > \alpha\sqrt{\sigma_o^2 + \sigma_b^2}. \tag{7}$$

Here, d represents one scalar element from the departure vector $\mathbf{d}_\mathrm{i}$ (Eq. 2). This check is applied during the FG trajectory. For all-sky observations, σ_o is the observation error (Eq. 6). α is set to 2.5, in common with many other observation types. σ_b is an estimate of the background error in observation space. This is based on the temperature field and is of order 1 K, which is extremely unrealistic in cloudy and/or rainy areas. In further work we will make this more realistic, but for the moment, this very small σ_b is used to provide an overly stringent QC of the observations. This has the positive benefit of helping to avoid cases with strong nonlinearity, and represents a conservative initial approach to using the cloud and rain affected observations.

As mentioned earlier, a second procedure (VarQC, Andersson and Järvinen, 1998) operates during the 4D-Var minimisation. This is applied to most observations in the ECMWF system, including all-sky observations. VarQC applies a weight to each observation in the minimisation according to how well it agrees with surrounding data, as represented by the evolving analysis state during the minimisation. Observations are never truly 'rejected', but merely downweighted to the point where they are no longer relevant. As well as losing weight, observations may regain it again if the analysis (based mostly on other observations) starts to agree with the observation. Technically, this method is implemented by modifying the observation error distribution assumed in 4D-Var from a pure Gaussian to a Gaussian plus a constant representing the possibility of erroneous data.

Figure 5 shows histograms of SSM/I channel 19v FG departures for one analysis, divided into the samples that pass QC checks and those that are rejected. About 20,000 observations pass QC. BgQC acts essentially to reject all observations with FG departures greater than about 10 K: this is about 800 observations. The

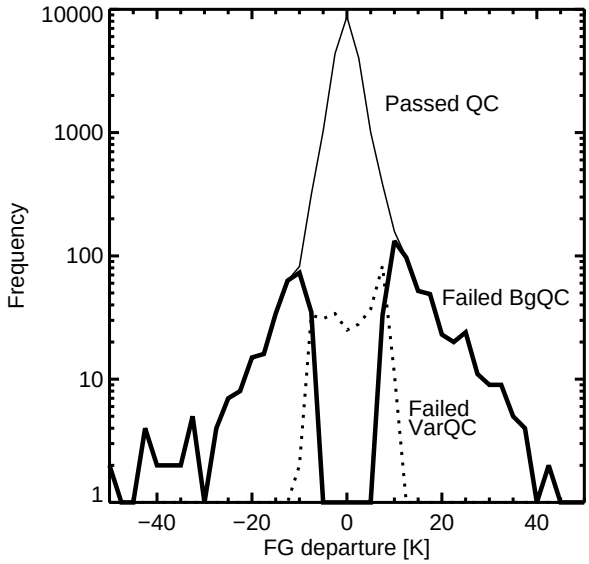

Figure 5: Histogram of SSM/I channel 19v FG departures from one analysis cycle, 00Z on 1st March 2009, showing the numbers that were rejected by BgQC or actively assimilated (thin line); rejected by BgQC (thick line); rejected by VarQC (dashed line).

observations rejected by BgQC are almost exclusively associated with rain and cloud systems, where the result of disagreement between observation and model can be large in TB terms. Observations which pass BgQC may still be affected by VarQC. Observations are flagged as 'failed' if they have been downweighted by at least 75%. VarQC 'rejects' a further 100 observations according to this measure. Again, these rejections tend to be in rainy and cloudy areas. Overall, our QC approach eliminates a large proportion of the observations in strongly rainy and cloudy areas. However, 95% of observations are still being used, which is a much larger proportion than in traditional 'clear sky' microwave imager assimilation (roughly 50% at ECMWF were considered clear). Hence, we can still justifiably refer to our approach as an 'all-sky' system.

We have so far only considered channel 19v, where the observation error is always quite small. The channel 19v results are valid also for 19h and 22v, where the observation error is similar. Channels 37v and 85v are given much larger observation errors in rain and cloud. Hence, BgQC does not reject many rain and cloud affected observations for these channels, but the high errors mean these observations have little impact.

4.4 Bias correction

Bias correction in the all-sky system is done by VarBC (Dee, 2004; Auligné *et al.*, 2007), which estimates bias correction coefficients as part of the 4D-Var assimilation. For the all-sky implementation we used the same predictors as the original clear-sky assimilation of microwave imagers. These are a constant, skin temperature, TCWV, surface wind speed, plus a 4-order polynomial of the scan position that accounts for scan biases. The second part of this paper (Geer *et al.*, 2010b) finds that globally, the VarBC system is capable of controlling the bias. However, at a local scale there are many biases associated with cloud and precipitation systems. To correct these we would need to add predictors based on the cloud or rain amount. For the first implementation of the All-Sky approach, we judged that these uncorrected biases could be tolerated, and they are generally much smaller than were found in the 1D+4D-Var system. This is due both to the more-accurate moist physics used in 4D-Var, and recent improvements in the treatment of cloud fraction in the radiative transfer model (Geer

et al., 2009). Nevertheless, improving the bias correction is a high priority for the future.

4.5 Spatial representativeness

Representativity issues are largely neglected in clear sky assimilation, but in cloud and rain they become much more important. The SSM/I field of view (FOV) is 45 km × 70 km at 19 GHz and 25 km × 35 km at 37 GHz. The model grid box size is roughly 25 km × 25 km at T799. These are all close enough that the SSM/I field of view and model grid-boxes are assumed to be equivalent. This appears to have worked well both for the 1D+4D-Var rain assimilation and for the new system.

AMSR-E has a much smaller field of view than SSM/I, being 16 km × 27 km at 19 GHz and 8 km × 14 km at 37 GHz. Using AMSR-E in the 1D+4D-Var system we ignored this and found no problems in doing so. We tried to do the same in the all-sky 4D-Var system, but we found forecast score degradations at short ranges (T+12 to T+48) in trade cumulus areas in the N. and S. Atlantic and in the Pacific. These areas can exhibit scattered cloudy, rainy and clear areas with variations on scales that are too small to be represented by the model, let alone forecast accurately. It appeared that by attempting to assimilate some of this variability, we were bringing unwanted noise into the analysed moisture and temperature fields. Hence we introduced a 'superobbing' of AMSR-E data.

Superobbing, as implemented here, simply averages the nearest 10 observations to the outer-loop grid point, with no observation allowed to be further than 20 km from the grid point. The AMSR-E superob is intended to have a spatial resolution closer to that of SSM/I. We found that when superobbing was implemented, the forecast degradations in trade cumulus areas were largely removed.

We are aware that even with the superobbing of AMSR-E, our treatment of representativity is currently quite superficial. Improvements in this area may bring substantial benefits to the system and we aim to revisit this in the future.

5 Single-observation tests

5.1 Introduction

To illustrate the way the new system works, we can run a full 4D-Var analysis, but assimilate only one observation. The FG is the same in all cases. We present the following examples:

- **A:** Convection in the inter-tropical convergence zone (ITCZ): model has too much rain compared to the observation (Tab. 1);
- **B:** Midlatitude cold front: model has too little moisture and cloud (Tab. 2).
- **C:** Convection in the ITCZ: a near neighbour to case A, but chosen to illustrate a situation with poor minimisation quality. No table is given, but the case is examined in Sec. 5.3. Coordinates: 1.9 °N, 24.2 °W. Time: 18:47 Z 30 Sep 2007.

For both FG and analysis, the tables list the departures (Eq. 2) and the values of TCWV and total column hydrometeor amount at the observation point and time. Each case has been run with three different assimilation methods:

Table 1: Single-observation case A (1.9°N, 24.2°W, 18:47 Z 30 Sep 2007.).

	FG	Analysis		
		All-sky-1	All-Sky-2	1D+4D-Var
Departures [K]				
19v	-6.9	-5.7	-1.5	-1.8
19h	-12.6	-10.4	-2.1	-2.7
22v	-3.3	-2.7	-1.5	-1.8
37v	-9.3	-7.3	-8.4	-12.4
37h	-26.8	-22.3	-18.6	-26.4
85v	14.6	14.8	4.3	4.8
85h	9.7	10.8	0.2	-4.5
Total columns [kg m^{-2}]				
TCWV	59.5	59.2	57.7	58.0
CWP	0.19	0.17	0.21	0.28
IWP	0.19	0.16	0.10	0.12
RWP	0.35	0.32	0.18	0.17
SWP	1.07	1.06	0.22	0.23

Table 2: Single-observation case B (40.6°N, 52.6°W, 20:40 Z 30 Sep 2007.)

	FG	Analysis		
		All-sky-1	All-Sky-2	1D+4D-Var
Departures [K]				
19v	7.6	7.4	3.3	5.6
19h	10.4	9.9	2.3	6.5
22v	9.8	9.1	0.8	5.2
37v	9.3	9.1	6.4	8.1
37h	16.2	15.7	8.8	13.0
85v	10.4	10.4	8.8	10.3
85h	22.2	21.5	11.3	17.0
Total columns [kg m^{-2}]				
TCWV	17.3	17.7	23.6	18.9
CWP	0.01	0.01	0.03	0.02
IWP	0.19	0.19	0.23	0.23
RWP	0.00	0.00	0.00	0.00
SWP	0.45	0.49	0.80	0.67

- **All-sky-1:** Uses the exact operational implementation;
- **All-sky-2:** As above, but 'unrestricted' - inflation of observation error with distance (Eq. 6) has been turned off, as has quality control (both BgQC and VarQC);
- **1D+4D-Var:** Uses the previous operational system, but again quality control has been turned off. The departures given in Tabs. 1 and 2 are based on 4D (not 1D) model calculations, for consistency with the All-Sky experiments. Bias corrections from the All-Sky-1 approach have been applied to these departures, since the 1D-Var bias corrections would not be appropriate.

5.2 Analysis quality

In the ITCZ example (case A, Tab. 1), FG TBs are too high compared to observations and there are negative FG departures in channels 19v to 37h. Thus the model has too much TCWV, cloud or rain. In All-Sky-1, All-Sky-2 and 1D+4D-Var approaches, the nominal observation errors for channels 19v, 19h and 22v are set to 3, 6 and 3 K respectively. 1D+4D-Var does not use the higher frequency channels at all. In the all-sky approach, the presence of heavy precipitation and cloud in the FG leads to observation errors for the 37 GHz and 85 GHz channels greater than 100 K, meaning these channels are effectively unused (see Sec. 4.2). In no case does BgQC reject the observation. Hence, observation errors and channel usage are identical in all three methods, except that All-Sky-1 adds an inflation term for the observation error (Eq. 6).

In the analysis, all three approaches reduce the departures, but in the new operational approach (All-Sky-1), the reduction is not large. The impact of the observation is much larger in All-Sky-2 and the analysis departures become quite small. A good fit to observations has been achieved by decreasing water vapour in the model (TCWV goes from 59.5 to 57.7 kg m^{-2}) and rain (RWP goes from 0.35 to 0.18 kg m^{-2}). This has been achieved by reducing the strength of convection in this profile. Figures 6b, c and d show how the vertical profiles of humidity, cloud and rain have been changed at the observation point. Snow is also reduced (SWP goes from 1.07 to 0.22 kg m^{-2}) and the impact of this is seen in the high-frequency channels (85v and 85h) where scattering from falling snow typically depresses TBs. Here, positive FG departures indicate excess snow, which is then corrected in the analysis. To achieve reduced convection at the observation time, the 4D-Var analysis has adjusted moisture in the lower and mid troposphere at the start of the analysis window (09Z, Fig. 6a).

The lack of observational impact in the All-Sky-1 approach comes from using much larger effective observation errors than in All-Sky-2. As the inner loop resolution increases from T95 to T159 to T255, the distance of this observation from the nearest model grid point is 99, 65 and 39 km respectively. As a result, observation error is inflated by 98.2 K, 41.7 K and 15.6 K respectively. It is clear that very little weight will be given to an individual observation in this case.

The 1D+4D-Var approach produces a very similar result to All-Sky-2. One justification for moving to a 4D-Var approach was that assimilating just a TCWV pseudo-observation might not be sufficient to change the cloud and rain fields appropriately. For this case at least, the 1D+4D-Var approach is perfectly effective, and directly assimilating TBs provides little improvement. In fact, because of the error inflation with distance in All-Sky-1, a single observation will typically have much lower weight in the new system than in the old. However, in the normal operational context, this 1D-Var observation would actually have been removed by quality control, due to an excess of falling snow compared to rain (Geer *et al.*, 2007).

Case B (Tab. 2) illustrates a midlatitude frontal situation. The front is indicated by a band of high TCWV running from SW to NE across a section of the N. Atlantic. Low TCWV to the NW indicates cold, dry air behind the front. At the observation point, the FG has too little water vapour and cloud, resulting in positive

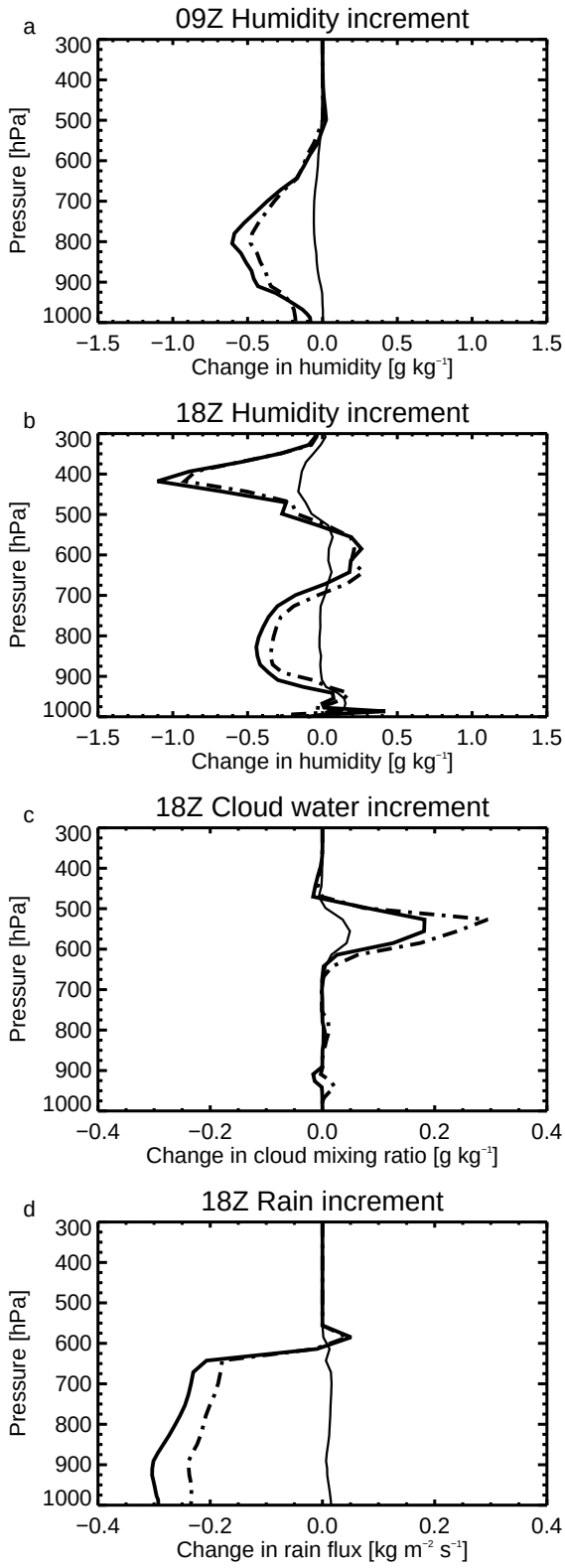

Figure 6: Single-observation case A: Vertical profiles of humidity and cloud water increments at the observation point: (a) Specific humidity at 09Z; (b) Specific humidity at 18Z; (c) cloud water mixing ratio at 18Z; (d) Rain flux at 18Z. Cloud and rain increments at 09Z are so tiny that they are not worth showing. Thin solid line: All-Sky-1; Thick solid line: All-Sky-2; Dot-dash line; 1D+4D-Var

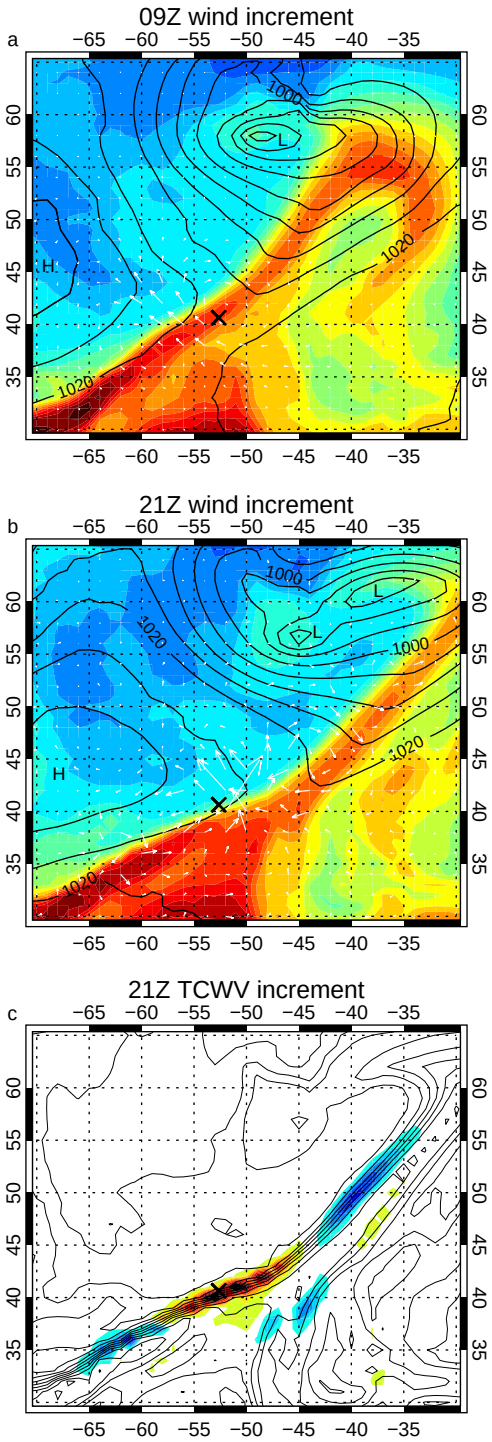

Figure 7: Single-observation test case B, using the All-Sky-2 approach: (a) 09Z and (b) 21Z wind increments at 670 hPa (white arrows) over FG sea-level pressure (black lines, 5 hPa contour spacing) and TCWV (coloured contours, blue = low; red = high); (c) 21Z TCWV increments (red is an increase; blue is a decrease; extremes are approximately +2kg m^{-2} and -1kg m^{-2}) over FG TCWV (black lines, 4 kg m^{-2} contour spacing; this is the same field that is shown in panel b). Colour bars have been omitted in order to simplify the diagram. X marks the location of the assimilated observation, which was valid at 20:40Z. 09Z TCWV increments are so small that there is no point showing them: the principal change at 09Z is in the winds, temperature and pressure .

FG departures. TCWV and CWP are increased in the analysis so that modelled TBs become higher and the analysis departures become smaller. Again, observation impact is small in All-Sky-1 and it is necessary to turn off the observation error inflation (All-Sky-2) in order to see the maximum potential impact of the observation. However, this time 1D+4D-Var has less impact than All-Sky-2, which may happen because a direct radiance analysis must adjust both cloud water and humidity to fit the observations, whereas in 1D+4D-Var, the analysis only needs to adjust the humidity.

Figure 7 shows the increments in the All-Sky-2 analysis. In contrast to the tropical case (A), where increments were localised and limited to the moist variables, case B involves changes to the large-scale wind fields and (not shown) temperature and pressure. Winds near the observation location are roughly NW (not shown). Wind increments act to decrease the wind speed by roughly 1 m s^{-1} at the beginning of the assimilation window (panel a), thus slowing down the progress of the front and increasing the humidity at the observation time and location (panels b and c). There is virtually no humidity increment at the beginning of the assimilation window. Because the background error formulation includes a constraint to ensure that any increments are in geostrophic balance, the local decrease in the wind field is associated with a dipole change in the pressure fields, filling in the low pressure area and reducing the high pressure area (not shown). Another result is that these pressure changes are also associated with an increase in wind speed on the outside of the dipole.

TCWV changes near the observation time (Fig. 7c) are associated with the steep gradients in the TCWV field. Where the progress of the front has been retarded, this results in an increase, and where it has been speeded up, this results in a drop in TCWV. There are smaller decreases in the TCWV on the forward side of the front where the TCWV gradient is steep. The 'tracer effect' of assimilating observations sensitive to humidity has also been shown by e.g. Peubey and McNally (2009).

In summary, the single-observation tests show that direct 4D-Var assimilation is able to adjust dynamical, moisture and cloud and precipitation fields in order to match the all-sky observations. The inflation of observation error with distance from the grid points means that the influence of any single observation will be quite low in the All-Sky-1 approach. Nevertheless, when all microwave imager observations are assimilated in the full system, the dynamical impact matches the previous approach, and the humidity constraint is roughly half as strong (Geer *et al.*, 2010b).

5.3 Minimisation quality

Single-observation tests also help illustrate the performance of the 4D-Var minimisation in the presence of the strong nonlinearities associated with cloudy and rainy observations. As we will see, incremental 4D-Var generally works well.

First we must outline how the incremental method is implemented at ECMWF. The outer-loop starts with a run of the non-linear forecast model from the background state to give $M_i[\mathbf{x}^{\mathrm{b}}(t_0)]$, the state about which the linearisations $\mathbf{H}$ and $\mathbf{M}_i$ are calculated. The inner loop is a variational minimisation which solves a linearised version of the cost function shown in Eq. 1. The inner loop solution is taken as the starting point for the next non-linear outer loop run. This is usually expressed in terms of an increment $\delta\mathbf{x}$ which is added to the original background state so the new outer loop calculates $M_i[\mathbf{x}^{\mathrm{b}}(t_0) + \delta\mathbf{x}]$. Whether the linear solution is valid depends on the validity of the tangent linear hypothesis (Eq. 3). Typically, the smaller $\delta\mathbf{x}$, the more valid this assumption. The idea of the incremental method is that the non-linear 'outer-loop' state becomes closer to the solution of the non-linear cost function and each successive increment $\delta\mathbf{x}$ is smaller than the last. In the operational system there are three steps in the outer loop and hence also three inner loop minimisations.

We will examine only the All-Sky-2 single-observation tests here, i.e. those performed without the usual restrictions of observation error inflation and QC, known as an 'unrestricted' approach (see Sec. 5.1). Hence,

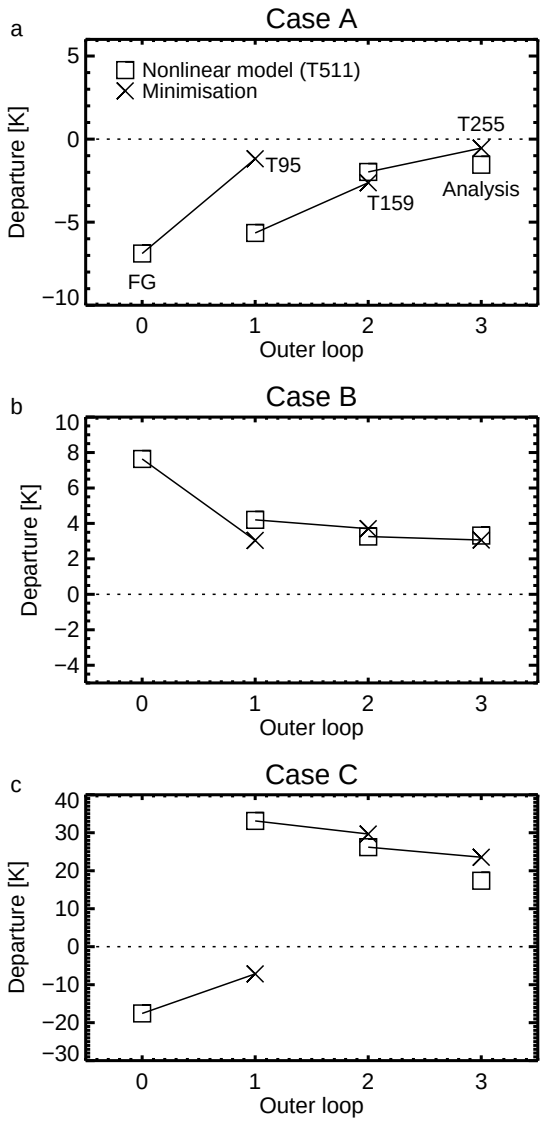

Figure 8: Channel 19v first guess departures through the 4D-Var minimisation for single-observation test cases A, B and C using the All-Sky-2 approach. Squares indicate departures calculated using the nonlinear T511 forecast model in the 'outer loop'; crosses indicate the departure at the end of each minimisations or 'inner loop', calculated using the incremental method. We do not show the intermediate departures during the inner-loop minimisation; the straight solid lines are simply illustrative.

the observations have a much larger impact than they usually would.

Figure 8 follows the channel 19v departures through the minimisation process. Looking at Case A, we see FG departures of -7K (see also Tab. 1), which have been generated from a run of the full nonlinear model at T511. Then, an inner-loop is run using the tangent-linear (TL) and adjoint models at T95. After a preset 70 iterations, the departure has been reduced to -1 K. This departure d_1' has been computed using the incremental approach, i.e. it is based on the TL model and observation operators **M** and **H**:

$$d_1' = y^{\mathrm{o}} - H[M[\mathbf{x}^{\mathrm{b}}(t_0)]] - \mathbf{HM}\delta\mathbf{x}_1. \tag{8}$$

For notational simplicity we have dropped the timestep indicator i from the model M. We are thinking about just a single observation y^{o}, i.e. this is a scalar here, as is the nonlinear observation operator H. $\delta\mathbf{x}_1$ is the increment generated by the first inner loop.

A second full-resolution nonlinear trajectory (outer-loop) now runs to compute the cost function with this increment. The corresponding nonlinear departure d_1 is:

$$d_1 = y^{\mathrm{o}} - H[M[\mathbf{x}^{\mathrm{b}}(t_0) + \delta\mathbf{x}_1]] \tag{9}$$

Figure 8a shows that this is -6 K. This suggests that the TL assumption (Eq. 3) is invalid, although the resolution mismatch between outer loop and inner loop (T511 vs. T95) is very large and likely also causes problems. In geophysical terms, the increment $\delta\mathbf{x}_1$ is able to reduce TCWV, cloud and rain at the observation point when fed through the T95 TL model, but it is largely ineffective in the T511 nonlinear model. However the incremental approach exists in order to deal with such non-linearities.

A second inner loop is run, which reduces the departure to -2 K. This is based on a new increment, $\delta\mathbf{x}_2$:

$$d_2' = y^{\mathrm{o}} - H[M[\mathbf{x}^{\mathrm{b}}(t_0) + \delta\mathbf{x}_1]] - \mathbf{HM}\delta\mathbf{x}_2. \tag{10}$$

This time the nonlinear departure,

$$d_2 = y^{\mathrm{o}} - H[M[\mathbf{x}^{\mathrm{b}}(t_0) + \delta\mathbf{x}_1 + \delta\mathbf{x}_2]], \tag{11}$$

is much smaller, also approximately -2 K. This shows that the nonlinearity has lessened. It is also likely that the increase in resolution of the TL model to T159 has helped. The final inner loop is run at T255 and manages to reduce the departure a little further, to -1 K, and the true analysis departure, computed using a final run of the nonlinear model, is relatively close, at -1.5 K. Hence, this example shows the incremental 4D-Var approach can deal quite successfully with the nonlinearities inherent in a convective situation.

Case B (Fig. 8b; Tab. 2) illustrated a midlatitude frontal situation. This appears to suffer far less from nonlinearity or resolution effects, with the linear and nonlinear departures being relatively close. Most of the work appears to be done in the first minimisation. We would not expect the departure to go to zero, as the assimilation will strike a balance between the background and observational information. Again, incremental 4D-Var seems to work well.

Case C has been chosen to illustrate a more problematic situation. This is a convective case with heavy rain and cloud in the FG (4.2 and 4.0 kg m^{-2} respectively). The observation disagrees, and a FG departure of -18 K shows that rain and cloud amounts should be much lower. The first inner loop is able to reduce this departure, but when these increments are fed into the nonlinear model, convection is switched off and cloud and precipitation nearly disappear (not shown). The new departure is +32 K. Further inner loop minimisations are unable to reverse this, and the analysis departure is as large as the FG departure, but with opposite sign.

However, in the normal All-Sky system, we place greater restrictions on the use of rainy and cloudy observations. In practice, Case C would have been rejected by QC (Sec 4.3) because the FG departures are much

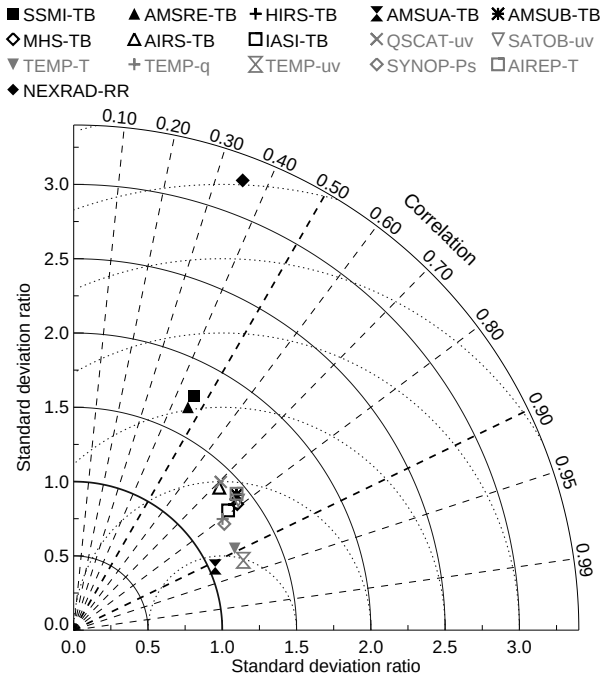

Figure 9: Taylor diagram showing statistics of inner loop departures $\mathbf{d}'_1$ versus outer loop departures $\mathbf{d}_1$ in observation space from a single 12-hour 4D-Var assimilation cycle at 0000 UTC 1 April 2009. Each observation type and measured variable is shown with a different symbol, as described in the legend. Correlation is measured in azimuth while standard deviation ratio is shown in the radial direction. The perfect match would be found at the point for which correlation and standard deviation ratio are both equal to 1. The further away from this point, the worse the agreement between $\mathbf{d}'_1$ and $\mathbf{d}_1$ and the less valid is the tangent linear assumption.

larger than would be expected given the observation error. If such an observation did get through BgQC, VarQC would act to downweight its influence in the analysis due to the continuing large departures.

These test cases suggest that incremental 4D-Var usually works well at dealing with nonlinearity and that in situations where it might not, observations will be rejected by quality control.

6 Convergence and performance in full system

6.1 Nonlinearity in observation space

We can also investigate nonlinearity in the context of the full observing system. Here we look at a single 12-hour 4D-Var assimilation cycle at 0000 UTC 1 April 2009 using the ECMWF operational configuration. For illustrative purposes we have also included some experimental, passively monitored surface rain radar observations.

Figure 9 displays a Taylor diagram comparing the inner loop departures $\mathbf{d}'_1$ (Eq. 8, vectorized) with the corresponding outer loop departures $\mathbf{d}_1$ (Eq. 9) after the first minimisation for the main observation types assimilated in the ECMWF 4D-Var. Essentially, this comparison represents a test of the tangent linear hypothesis, including the use of a lower resolution in the linearised model. Each symbol represents a given observation type and its location on the diagram gives both the correlation (in azimuth) and the standard deviation ratio (radial distance;

Table 3: Acronyms of satellite observation types in Figs. 9 and 10

Acronym	Description
HIRS	High Resolution Infrared Radiation Sounder
AMSU-A	Advanced Microwave Sounding Unit A
AMSU-B	Advanced Microwave Sounding Unit B
MHS	Microwave Humidity Sounder
AIRS	Advanced Infrared Sounder
IASI	Infrared Atmospheric Sounding Interferometer
QuikSCAT	Quick Scatterometer

SDR hereafter). Ideally, a perfect match would be obtained for a correlation and an SDR value both equal to 1 (inner loop departures, $\mathbf{d}'_1$, being chosen as the reference here). It should also be noted that in Fig. 9 all assimilated channels of a given instrument have been combined in the statistics. Observation types consist of polar orbiting satellite measurements (SSM/I, AMSR-E, HIRS, AMSU-A, AMSU-B, MHS, AIRS, IASI TBs, QuikSCAT wind - see Table 3 for acronyms not yet defined), geostationary satellite wind vectors (SATOB-uv), radiosonde temperature, specific humidity and wind measurements (TEMP-T, TEMP-q and TEMP-uv), surface pressure data (SYNOP-Ps) and aircraft temperature reports (AIREP-T).

Figure 9 clearly demonstrates that all observation types that are not directly affected by clouds and precipitation exhibit an SDR between 1.05 and 1.45 and a correlation coefficient ranging between 0.7 and 0.93, which is far from perfect but still reasonable. For most observation types, the correlation is around 0.8, while the highest values are obtained for AMSU-A TBs (mainly sensitive to temperature) and temperature and wind radio-soundings (TEMP-T and TEMP-uv). On the other hand, for SSM/I and AMSR-E TBs, which are often strongly affected by clouds and precipitation, the correlation coefficient drops to about 0.46 and SDR increases to 1.7, some distance away from all other observation types. As further evidence of the degradation of the validity of the linear assumption for precipitation observations, the statistics for hourly rain rate observations from the network of ground-based precipitation radars over the U.S.A. (NEXRAD-RR) are also plotted in Fig. 9. For these observations, the match between increments from minimisation and trajectory becomes even worse since correlation drops to 0.35 while SDR reaches 3.25.

As a general remark, Fig. 9 shows that for all observation types, SDR values are always larger than 1, which points towards a systematic underestimation of increment sizes in the linear computations of the minimisation or a systematic (spurious) amplification in the nonlinear calculations of the trajectory. It is also found that the linearity assumption in observation space becomes less valid for most observation types away from the beginning of the assimilation window (not shown).

The Taylor diagram for the third (and final) minimisation is displayed in Fig. 10. It shows that statistics are improved compared to the first minimisation as a result of the reduced resolution gap between third minimisation and trajectory, and also because of the usually smaller magnitude of increments/departures.

An additional Taylor diagram is plotted for individual channels of SSM/I and AMSR-E in Fig. 11. The highest correlations and SDR values closest to unity are obtained for channels 22v of SSM/I and 24v and 24h of AMSR-E, which are mainly sensitive to moisture. The worst match (correlation below 0.4; SDR higher than 2.25) is found for the 37v channels of SSM/I and AMSR-E, which are highly sensitive to clouds and precipitation and therefore more subject to nonlinearities. Channels 19v and 19h lie in-between those two extremes as a result of their mixed sensitivities to moisture and hydrometeors.

This statistical comparison therefore confirms that for observations affected by clouds or (worse) precipitation, increments produced in the minimisations are quite often not translated into consistent increments in the fol-

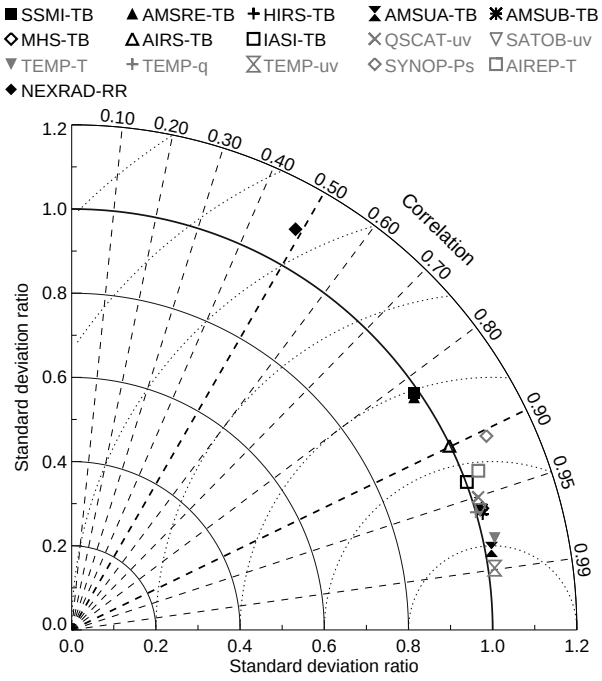

Figure 10: As for Fig. 9 but for the third and final minimisation.

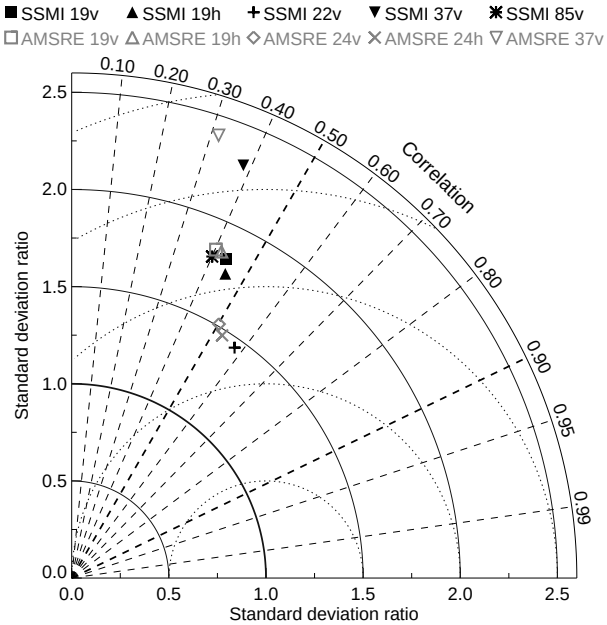

Figure 11: As for Fig. 9 but for individual AMSR-E and SSM/I channels.

Table 4: Number of iterations in each inner loop minimisation (mean for September 2007).

Outer loop	Control	All-Sky	Difference significant at [%]
1st	70.0	70.0	(fixed)
2nd	28.8	28.5	94
3rd	32.1	31.6	92

lowing high-resolution nonlinear trajectory. However, this problem becomes much smaller as the outer loop progresses, showing the incremental formulation appears to work reasonably well in reducing non-linearity. We would conclude that while the all-sky microwave imager observations are more non-linear than typical clear sky observations, they are sufficiently linear that it is valid to assimilate them operationally.

It is interesting to contrast this with the results of Marécal and Mahfouf (2003) who performed single-observation tests with rainfall observations in incremental 4D-Var. They observed big jumps in the value of the cost function between inner and outer loops (the departures, of course, make up part of the cost function - see Eq. 1) which they also ascribed to the inherent non-linearity of the situation. They concluded that direct 4D-Var of rainfall observations would be very tricky. However, the results of Geer *et al.* (2010b) show that direct 4D-Var appears to be working well. This is likely for the following reasons:

- All-sky microwave imager observations are not 'pure' rain observations - they are also sensitive to more linear quantities like TCWV and cloud;
- We have the benefit of moist physics parameterizations that have been carefully linearised (Tompkins and Janisková, 2004; Lopez and Moreau, 2005), specifically to avoid the kind of problems encountered by Marécal and Mahfouf;
- The analysis includes the full observing system, which means that the large scale wind and temperature fields are strongly constrained. This helps guide incremental 4D-Var towards the right solution, and means that in later inner loops, the size of the necessary increments $\delta\mathbf{x}$ is relatively small, i.e. the tangent linear approximation will become increasingly valid.
- A very cautious quality control eliminates contentious observations (see Sec. 4.3).

6.2 Minimisation quality

We can also examine whether the nonlinearity inherent in all-sky observations affects general measures of minimisation quality. The number of iterations needed in each inner-loop is shown in Tab. 4. The number is fixed to 70 in the first inner-loop but flexible in the second and third; these minimisations stop when convergence criteria have been satisfied. Here we use the Control and All-Sky experiments described by Geer *et al.* (2010b), which were run for a period of several months. The effect of going from Control to All-Sky is very small and, surprisingly, the number of iterations is reduced to a statistically significant degree. Practically, we would say that 4D-Var is working just as well as before.

Another thing to examine is the condition number, which is the ratio of the largest to the smallest eigenvalue of the Hessian of the cost function. This is a measure of the ill-conditioning of the inversion problem that is solved in the analysis. As shown in Fig. 12 it is in general little affected by the move to all-sky assimilation. There are isolated cases in the 2nd and 3rd trajectories where for one or two cycles the condition number is much higher than normal. However, these are just as likely to be found in the Control as in the All-Sky experiment, and they are probably associated with a particular synoptic situation on these days making it hard

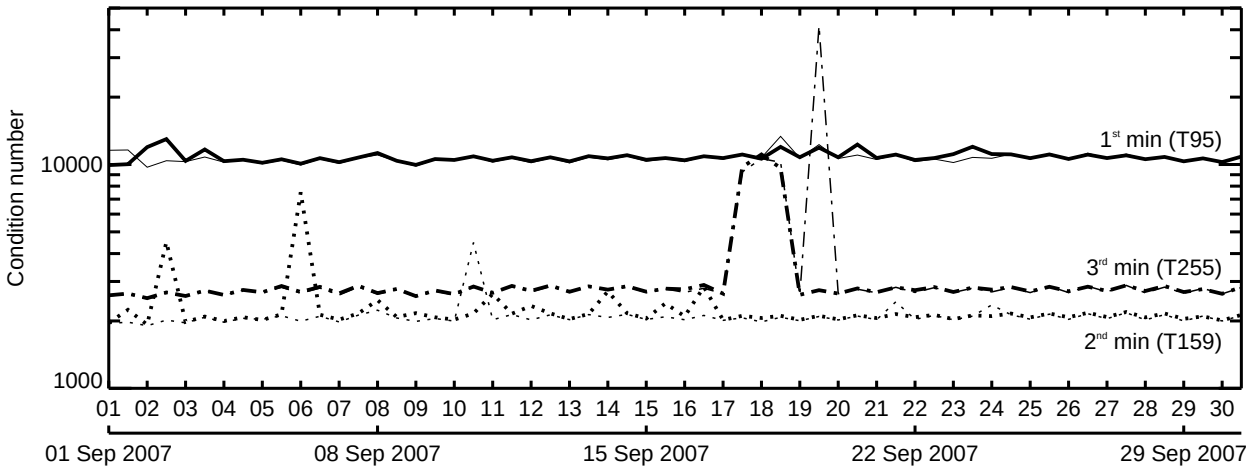

Figure 12: Condition number of each minimisation, against day. Thick line is Control; Thin line is All-Sky.

Table 5: Computer billing units for variational assimilation (mean for September 2007).

	First trajectory	Inner loops	Other trajectories
All-Sky	352	4002	1157
Control	661	3496	1208
No microwave imagers	327	3460	1101

for the minimisation to converge. All-Sky shows one particularly large peak in the 3rd minimisation, on 19th September. However, in our experience this can sometimes also happen in Control-type experiments, so we do not believe it is significant.

6.3 Numerical performance

The all-sky 4D-Var approach needed to be computationally efficient to be included as part of the ECMWF operational assimilation system. Table 5 shows the mean computational cost of variational assimilation for the All-Sky and Control experiments and for an experiment with all microwave imager assimilation switched off. Compared to this, the first trajectory of Control is much slower, since this is where the 1D-Var retrievals were run. However, 1D+4D-Var required little extra computation elsewhere, and direct assimilation of clear radiances was comparatively fast. In contrast, most of the cost of the All-Sky approach is in the inner loop minimisations. This is due to the use of scattering radiative transfer in the observation operator, and by the need to use a message-passing approach to move observations between processors. Overall, All-Sky is only a little more expensive than Control. Microwave imager assimilation in All-Sky has a cost equal to 13% of that of the no-imager reference, compared to 10% for Control.

Many actions were taken to make the cost of All-Sky comparable to that of Control, with the most significant being:

- A decision not to actively assimilate TMI and SSMIS observations. This was justified in part by the additional difficulties involved in using these particular instruments (Geer *et al.*, 2010a; Bell *et al.*, 2008).
- In the minimisations, TL and adjoint radiative transfer calculations are turned off for channels where the

observation error is greater than 50 K. Tangent-linear or adjoint gradients are set to zero in this case.

- General code optimisation, such as improving the ordering of memory access.

Another action was to turn off scattering radiative transfer in 'clear sky' situations. However, because the moist physics parametrisations almost always produce a small background level of cloud or rain, very few first guesses are truly 'clear sky' and this approach saved little time overall. We hope to revisit this in the future, since there are a significant proportion of atmospheric situations where full scattering radiative transfer should not be necessary, particularly at lower microwave frequencies.

7 Conclusion

A new system has been developed at ECMWF to assimilate radiances from passive microwave imaging radiometers such as SSM/I, AMSR-E and TMI. For the first time, it exploits the sensitivity of these radiances to temperature, water vapour, sea-surface wind, clouds and precipitation in all sky conditions. This is achieved through the use of a multiple-scattering radiative transfer model and the full set of moist physics parameterizations at all stages of the 4D-Var assimilation, i.e. wherever the cost function or its gradient is required. The unified treatment of radiances in clear-sky and cloud-affected regions permits a much improved balance of observational data usage in the analysis because it allows the active generation, dissipation and modification of clouds and clear sky conditions in consistency with the NWP model and the observations. It also overcomes the lopsided data usage towards clear-sky areas that is applied to most other satellite data types.

This paper presents the technical implementation of the system and a performance analysis focusing on the main issues related to radiance assimilation in clouds and precipitation: observation operator accuracy, observation error definition and bias correction, basic observational impact, 4D-Var linearity and stability as well as computational cost. The companion paper (Geer *et al.*, 2010b) addresses the impact of the new system in the full operational assimilation and prediction context.

Compared to a clear-sky data assimilation system roughly twice the number of observations are used. However, due to the difficulty of dealing with frozen precipitation at higher frequencies, only channels at 19 and 22/24 GHz are actively assimilated in cloud-affected areas. The new system dynamically adjusts observation operator errors as a function of the mass of hydrometeors in the atmospheric column and the distance between observation and model grid point location. Along with the use of VarQC, this gives a dynamic weighting of the observational impact as a function of atmospheric state. Tighter quality control and larger observation errors reduce the weight of microwave imager data in the assimilation compared to the previous system. However, the new approach is more balanced in terms of observation sampling.

Single-observation experiments demonstrate the mechanisms of the all-sky approach. Examples are shown both with and without the error inflation as a function of distance from the grid point. With error inflation, the observations have a weaker impact in the all-sky approach than in the previous 1D+4D-Var assimilation for cloudy and rainy areas. However, without error inflation, i.e. with identical observation errors used in each test, the all-sky analysis is closer to the observations than was possible with 1D+4D-Var. Even with a single observation significant wind increments can be produced in response to a disagreement between first-guess and observed moisture and cloud. Direct 4D-Var of rain and cloud affected observations allows a physically consistent adjustment of model dynamics with temperature and humidity increments, due to the sensitivity of the atmospheric state to radiance observations through the combined radiative transfer model and the moist physics parameterization.

The concern that minimisation performance would be poor when strongly non-linear models were employed ap-

pears unfounded. The incremental approach efficiently allows re-linearisation by running non-linear model updates between lower resolution minimisations. The single-observation tests demonstrated that the re-linearisation enables the minimisation to converge in most cases. Quality control is able to pick up situations where non-linearity remains an issue. The degree of non-linearity of the full 4D-Var operator has been calculated for all active observation types in the ECMWF assimilation system. While linearity of the operator for all-sky radiances is clearly inferior compared to other clear-sky satellite and also conventional observations, this discrepancy reduces between successive inner-loop minimisations. This is helped by the increase in spatial model resolution with each inner-loop and by the adjustment of large-scale dynamical structures in previous minimisations. The overall performance of the 4D-Var analysis remains unchanged, as indicated by the condition number and the number of iterations.

The new approach has a computational cost that is only a 3% higher than the previous system. This was achieved through the elimination of unnecessary observation operator calls, by reducing the number of satellites assimilated, and by computer code optimisation and parallelisation. The system has been run actively in the ECMWF forecasting system since March 2009.

Acknowledgements

Alan Geer was funded by the EUMETSAT fellowship programme. Gabór Radnóti is thanked for discussions on non-linearity and Jean-Noël Thépaut and Erland Källén are thanked for reviewing the manuscript.

References

Amerault C, Zou X. 2003. Preliminary steps in assimilating SSM/I brightness temperatures in a hurricane prediction scheme. *J. Atmos. Ocean Tech.* **20**: 1154–1169.

Amerault C, Zou X. 2006. Comparison between model-produced and observed microwave radiances and estimation of background error covariances for hydrometeor variables within hurricanes. *Mon. Wea. Rev.* **134**: 745–758.

Amerault C, Zou X, Doyle J. 2008. Tests of an adjoint model with explicit moist physics on the cloud scale. *Mon. Wea. Rev.* **136**: 2120–2132.

Andersson E, Bauer P, Beljaars A, Chevallier F, Hólm E, Janisková M, Kållberg P, Kelly G, Lopez P, Mcnally A, Moreau E, Simmons AJ, Thépaut JN, Tompkins AM. 2005. Assimilation and modeling of the atmospheric hydrological cycle in the ECMWF forecasting system. *Bull. Am. Met. Soc.* **86**: 387–402.

Andersson E, Järvinen H. 1998. Variational quality control. *ECMWF Tech. Memo., 250, available from http://www.ecmwf.int* .

Auligné T, McNally AP, Dee DP. 2007. Adaptive bias correction for satellite data in a numerical weather prediction system. *Quart. J. Roy. Meteorol. Soc.* **133**: 631–642.

Bauer P, Lopez P, Benedetti A, Salmond D, Moreau E. 2006a. Implementation of 1D+4D-Var assimilation of precipitation-affected microwave radiances at ECMWF. I: 1D-Var. *Quart. J. Roy. Meteorol. Soc.* **132**: 2277–2306.

Bauer P, Lopez P, Salmond D, Benedetti A, Saarinen S, Moreau E. 2006b. Implementation of 1D+4D-Var assimilation of precipitation-affected microwave radiances at ECMWF. II: 4D-Var. *Quart. J. Roy. Meteorol. Soc*. **132**: 2307–2332.

Bauer P, Moreau E, Chevallier F, O'Keeffe U. 2006c. Multiple-scattering microwave radiative transfer for data assimilation applications. *Quart. J. Roy. Meteorol. Soc.* **132**: 1259–1281.

Bell W, Candy B, Atkinson N, Hilton F, Baker N, Bormann N, Kelly G, Kazumori M, Campbell W, Swadley S. 2008. The assimilation of SSMIS radiances in numerical weather prediction models. *IEEE Trans. Geosci. Remote Sensing* **46**: 884–900.

Courtier P, Thépaut JN, Hollingsworth A. 1994. A strategy for operational implementation of 4D-Var, using an incremental approach. *Quart. J. Roy. Meteorol. Soc.* **120**: 1367–1387.

Dee D. 2004. Variational bias correction of radiance data in the ECMWF system. In: *ECMWF workshop proceedings: Assimilation of high spectral resolution sounders in NWP, 28 June – 1 July, 2004*. Eur. Cent. for Med. Range Weather Forecasts, Reading, UK, available from http://www.ecmwf.int, pp. 97–112.

Errico RM, Bauer P, Mahfouf JF. 2007. Issues regarding the assimilation of cloud and precipitation data. *J. Atmos. Sci.* **64**: 3785 – 3798.

Eyre JR. 1991. A fast radiative transfer model for satellite sounding systems. *ECMWF Tech. Memo., 176, available from http://www.ecmwf.int* .

Geer AJ, Bauer P, Bormann N. 2010a. Solar biases in microwave imager observations assimilated at ECMWF. *IEEE Trans. Geosci. Remote Sens.* : in press.

Geer AJ, Bauer P, Lopez P. 2007. Lessons learnt from the 1D+4D-Var assimilation of rain and cloud affected SSM/I observations at ECMWF. *Published simultaneously as ECMWF Technical Memoranda 535 and ECMWF/EUMETSAT fellowship reports 17* .

Geer AJ, Bauer P, Lopez P. 2008. Lessons learnt from the operational 1D+4D-Var assimilation of rain- and cloud-affected SSM/I observations at ECMWF. *Quart. J. Roy. Meteorol. Soc.* **134**: 1513–1525.

Geer AJ, Bauer P, Lopez P. 2010b. Direct 4D-Var assimilation of all-sky radiances: Part II. Assessment. *Quart. J. Roy. Meteorol. Soc., submitted* .

Geer AJ, Bauer P, O'Dell CW. 2009. A revised cloud overlap scheme for fast microwave radiative transfer. *J. App. Meteor. Clim.* **48**: 2257–2270.

Hollinger J, Peirce J, Poe G. 1990. SSM/I instrument evaluation. *IEEE Trans. Geosci. Remote Sensing* **28**: 781–790.

Ide K, Courtier P, Ghil M, Lorenc AC. 1997. Unified notation for data assimilation: Operational, sequential and variational. *J. Meteor. Soc. Japan* **39**: 2038–2052.

Ingleby NB, Lorenc AC. 1993. Bayesian quality control using multivariate normal distributions. *Quart. J. Roy. Meteorol. Soc.* **119**: 1195–1225.

Järvinen H, Unden P. 1997. Observation screening and background quality control in the ECMWF 3D-Var data assimilation system. *ECMWF Tech. Memo., 236, available from http://www.ecmwf.int* .

Joseph J, Wiscombe WJ, Weinman JA. 1976. The delta-Eddington approximation for radiative flux transfer. *J. Atmos. Sci.* **33**: 2452–2459.

Kalnay E. 2003. *Atmospheric modelling, data assimilation and predicatability*. Cambridge University Press.

Kawanishi T, Sezai T, Ito Y, Imaoka K, Takeshima T, Ishido Y, Shibata A, Miura M, Inahata H, Spencer R. 2003. The Advanced Microwave Scanning Radiometer for the Earth Observing System (AMSR-E), NASDA's contribution to the EOS for global energy and water cycle studies. *IEEE Trans. Geosci. Remote Sensing* **41**: 184–194.

Krishnamurti T, Ingles K, Cocke S, Pasch R, Kitade T. 1984. Details of low latitude medium range numerical weather prediction using a global spectral model, II: Effect of orography and physical initialization. *J. Meteor. Soc. Japan* **62**: 613–649.

Lopez P, Moreau E. 2005. A convection scheme for data assimilation: Description and initial tests. *Quart. J. Roy. Meteorol. Soc.* **131**: 409–436.

Marécal V, Mahfouf JF. 2003. Experiments on 4D-Var assimilation of rainfall data using an incremental formulation. *Quart. J. Roy. Meteorol. Soc.* **129**: 3137–3160.

Moreau E, Bauer P, Chevallier F. 2003. Variational retrieval of rain profiles from spaceborne passive microwave radiance observations. *J. Geophys. Res.* **108**: 10.1029/2002JD003 315.

Moreau E, Lopez P, Bauer P, Tompkins AM, Janisková M, Chevallier F. 2004. Variational retrieval of temperature and humidity profiles using rain rates versus microwave brightness temperatures. *Quart. J. Roy. Meteorol. Soc.* **130**: 827–852.

Peubey C, McNally A. 2009. Characterization of the impact of geostationary clear-sky radiances on wind analyses in a 4D-Var context. *Quart. J. Roy. Meteorol. Soc.* **135**: 1863 – 1876.

Rabier F, Järvinen H, Klinker E, Mahfouf JF, Simmons A. 2000. The ECMWF operational implementation of four-dimensional variational assimilation. I: Experimental results with simplified physics. *Quart. J. Roy. Meteorol. Soc.* **126**: 1148–1170.

Roberts N, Dean H. 2008. Scale-selective verification of rainfall accumulations from high-resolution forecasts of convective events. *Mon. Wea. Rev.* **136**: 78–96.

Saunders R. 2008. RTTOV-9 science and validation report. *NWP-SAF report NWPSAF-MO-TV-020, available from http://www.metoffice.gov.uk after requesting a password* .

Smith EA, Bauer P, Marzano FS, Kummerow CD, McKague D, Mugnai A, Panegrossi G. 2002. Intercomparison of microwave radiative transfer models for precipitating clouds. *IEEE Trans. Geosci. Remote Sensing* **40**: 541–549.

Tompkins AM, Janisková M. 2004. A cloud scheme for data assimilation: Description and initial tests. *Quart. J. Roy. Meteorol. Soc.* **130**: 2495–2517.

Treadon RE, Pan HL, Wu WS, Lin Y, Olson WS, Kuligowski RJ. 2002. Global and regional moisture analyses at NCEP. *Proc. workshop on Humidity Analysis, Reading, United Kingdom, ECMWF* : 33–47.

Tsuyuki T, Koizumi K, Ishikawa Y. 2002. The JMA mesoscale 4DVAR system and assimilation of precipitation and moisture data. *Proc. workshop on Humidity Analysis, Reading, United Kingdom, ECMWF* : 59–67.

Vukicevic T, Posselt D. 2008. Analysis of the impact of model nonlinearities in inverse problem solving. *J. Atmos. Sci.* **65**: 2803–2823.

Županski D, Mesinger F. 1995. Four-dimensional variational assimilation of precipitation data. *Mon. Wea. Rev.* **123**: 1112–1127.